Supplementary Information

Degradation pathways of penthiopyrad by δ-MnO_2 mediated processes: A combined density functional theory and experimental study

Ruishuang Xu[a,b]; Mengjiu Zhao[a]; Zhengqiang Chen[a]; Zhihong Gao[c]; Haiyan Song[a] *; Taicheng An[d]; Shengrun Zheng[a]; Fenglong Gu[a,b] *

[a] School of Chemistry, South China Normal University, Guangzhou 510006, PR China.

[b] Key Laboratory of Theoretical Chemistry of Environment, Ministry of Education; School of Chemistry, South China Normal University, Guangzhou 510006, PR China.

[c] Analysis and Testing Center, South China Normal University, Guangzhou 510006, PR China.

[d] Guangzhou Key Laboratory of Environmental Catalysis and Pollution Control, School of Environmental Science and Engineering, Institute of Environmental Health and Pollution Control, Guangdong University of Technology, Guangzhou 510006, PR China.

* Corresponding author: Haiyan Song; Fenglong Gu

E-mail: songhaiyan@m.scnu.edu.cn; gu@scnu.edu.cn

Tel.: 86-20-39310253; Fax: 86-20-39310187

This supplementary information include:

1) Text S1 Fukui function

2) Figures:

Fig. S17. Effect of metal cations on penthiopyrad degradation .

Fig. S18. (a) Effect of humic acid on penthiopyrad degradation; (b) FTIR spectra of the humic acid.

S1. Fukui function

Fukui function has been widely used to predict the reactive sites of electrophilic, nucleophilic, and radical attacking (Kong et al., 2020; Parr and Yang, 1984). Specifically, Fukui function is defined as:

$$f(r) = \left[\frac{\partial_\mu}{\partial_v(r)}\right]_N = \left[\frac{\partial_\rho(r)}{\partial N}\right]_{v(r)} \quad (1)$$

where $\rho(r)$ is the electron density at a point *r* in space, *N* is electron number in present system, the constant term *v* in the partial derivative is external potential. In the condensed version of Fukui function, atomic population number is used to represent the amount of electron density distribution around an atom. The condensed Fukui function can be calculated unambiguously for three situations:

Nucleophilic attack: $f_A^+ = q_N^A - q_{N+1}^A$ (2)

Electrophilic attack: $f_A^- = q_{N-1}^A - q_N^A$ (3)

Radical attack: $f_A^0 = (q_{N-1}^A - q_{N+1}^A)/2$ (4)

where q^A is the atom charge population of atom *A* at corresponding state. The Fukui function contains relative information about different sites of one molecule, and the reactive sites of the exact molecule usually have larger value of condensed Fukui function (CFF) than other regions.

References:

Kong, W., Gao, Y., Yue, Q., Li, Q., Gao, B., Kong, Y., Wang, X., Zhang, P. and Wang, Y., 2020. Performance optimization of CdS precipitated graphene oxide/polyacrylic acid composite for efficient photodegradation of chlortetracycline. J. Hazard. Mater. 388, 121780. https://doi.org/10.1016/j.jhazmat.2019.121780

Parr, Robert G. and Yang, W., 1984. Density functional approach to the frontier-electron theory of chemical reactivity. J. Am. Chem. Soc. 106, 4049-4050. https://doi.org/10.1021/ja00326a036

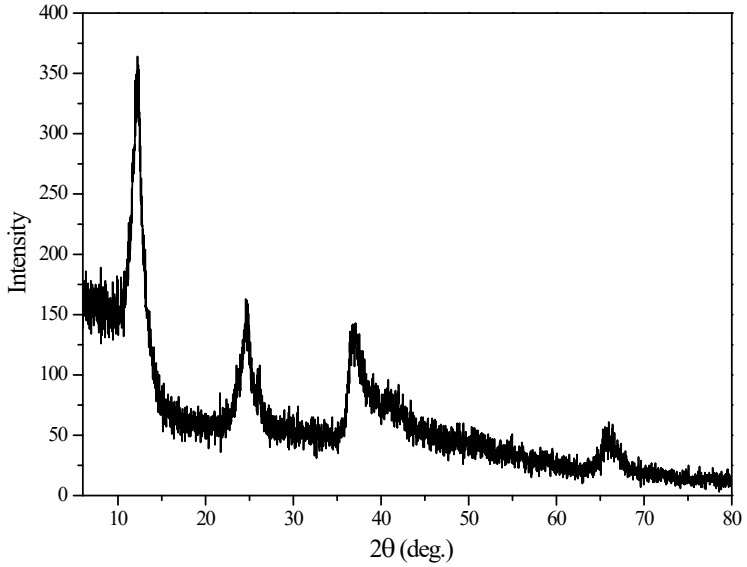

Fig. S1. X-ray diffraction pattern of the synthesized δ-MnO_2.

X-ray diffraction (XRD) determined the phase structures of the synthesized MnO_2 was present in Fig. S1. The diffraction peaks could be observed at 2θ =12.3, 24.6, and 36.9, which is precisely similar to that of δ-MnO_2 (Zhong et al. 2019), and the synthesized δ-MnO_2 sample was low crystallized.

References:

Zhong, C., Zhao, H., Cao, H., Fu, J., Xie, Y. and Sun, Z., 2019. Acidity induced fast transformation of acetaminophen by different MnO_2: Kinetics and pathways. Chem. Eng. J. 359, 518-529. https://doi.org/10.1016/j.cej.2018.11.172.

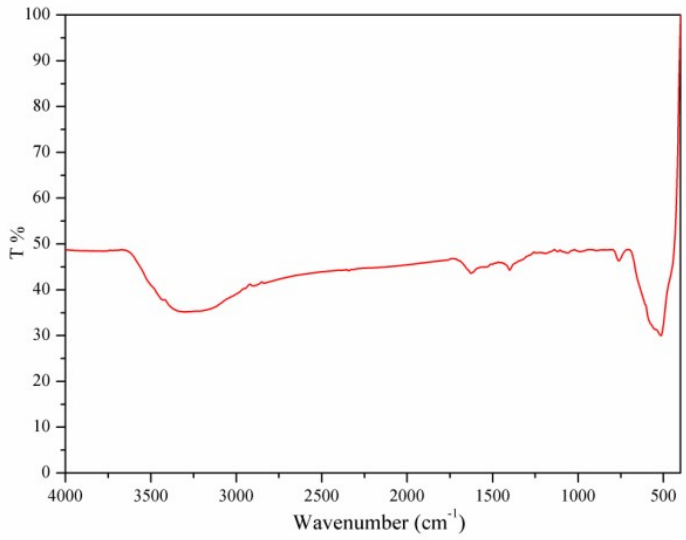

Fig. S2. FTIR spectra of the synthesized δ-MnO_2.

The functional groups of δ-MnO_2 was characterized in Fig.S2. The characteristic stretching vibration peak of the O-Mn-O bond appears near the wavenumber 510 cm^{-1} in FT-IR spectra , which confirms the existence of the MnO_2 unit cell (Li et al., 2017). The typical absorption band in the wavenumber range of 3600 to 3000 cm^{-1} corresponded to the stretching of O-H in water molecules and Mn-OH groups, and the absorption peak at 1624 cm^{-1} represents the bending vibration of Mn-OH. The simultaneous appearance of these peaks indicates that the sample contains bound water molecules.

References:

Li, L., Wei, D., Wei, G. and Du, Y., 2017. Product identification and the mechanisms involved in the transformation of cefazolin by birnessite (δ-MnO_2). Chem. Eng. J. 320, 116-123. https://doi.org/10.1016/j.cej.2017.03.021

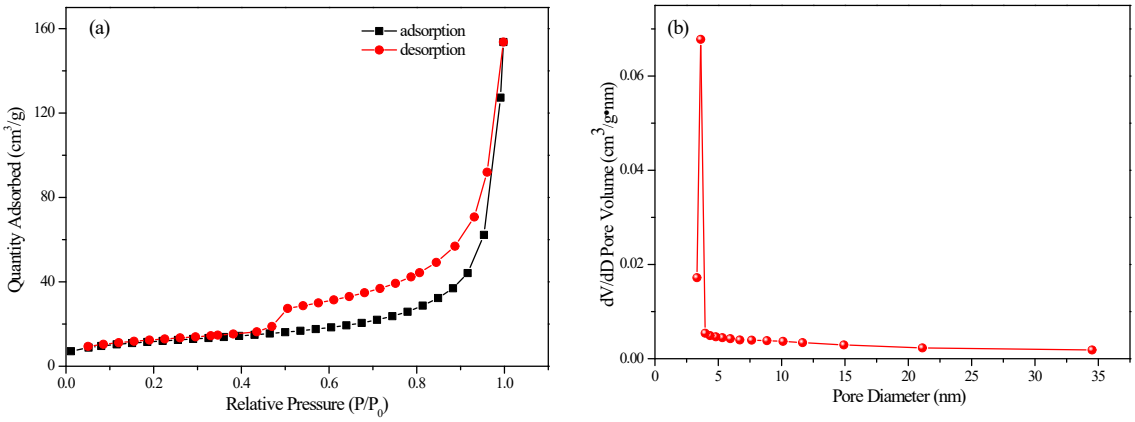

Fig. S3. N_2 adsorption-desorption isothermals and pore-size distribution curves of the δ-MnO_2.

The surface areas of the synthesized δ-MnO_2 was determined by N_2 adsorption-desorption isotherms in Fig. S3. The adsorption-desorption isotherms for the δ-MnO_2 sample was given in Fig. S3 (a), the Brunauer-Emmett-Teller (BET) surface area of the sample is determined to be 40.92 m^2/g. As shown in Fig. S3 (b), the pore size distribution was measured from the isotherm by the BJH model, which indicated that the narrow distribution is around mesopore region.

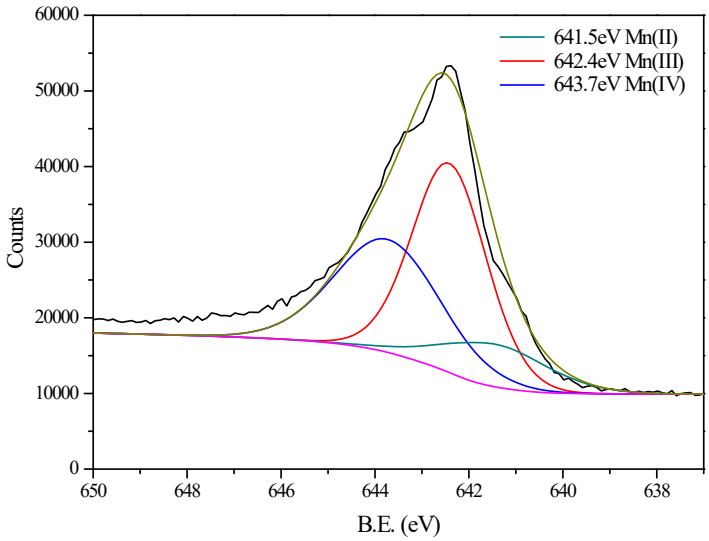

Fig. S4. The Mn $2p_{3/2}$ XPS spectra of the synthesized δ-MnO_2.

Fig. S4 shows the Mn $2p_{3/2}$ XPS spectra of the synthesized δ-MnO_2. The Mn $2p_{3/2}$ peak were deconvoluted into three peaks: Mn(IV) at 643.7 eV, Mn(III) at 642.4 eV and Mn(II) 641.5 eV according to reference (Zhong et al. 2019), the relative Mn content of different oxidation states was 37%, 49% and 14%, which indicated that Mn(III) > Mn(IV) >> Mn(II).

References:

Zhong, C., Zhao, H., Cao, H., Fu, J., Xie, Y. and Sun, Z., 2019. Acidity induced fast transformation of acetaminophen by different MnO_2: Kinetics and pathways. Chem. Eng. J. 359, 518-529. https://doi.org/10.1016/j.cej.2018.11.172.

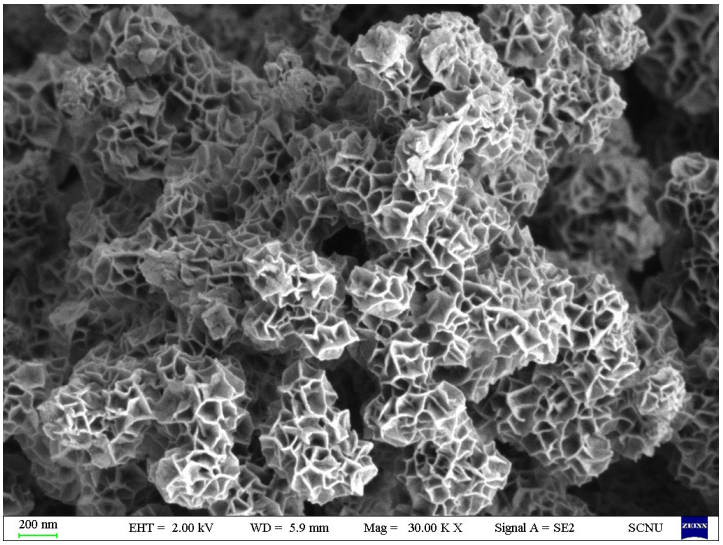

Fig. S5. SEM patterns of the flower-shape δ-MnO_2.

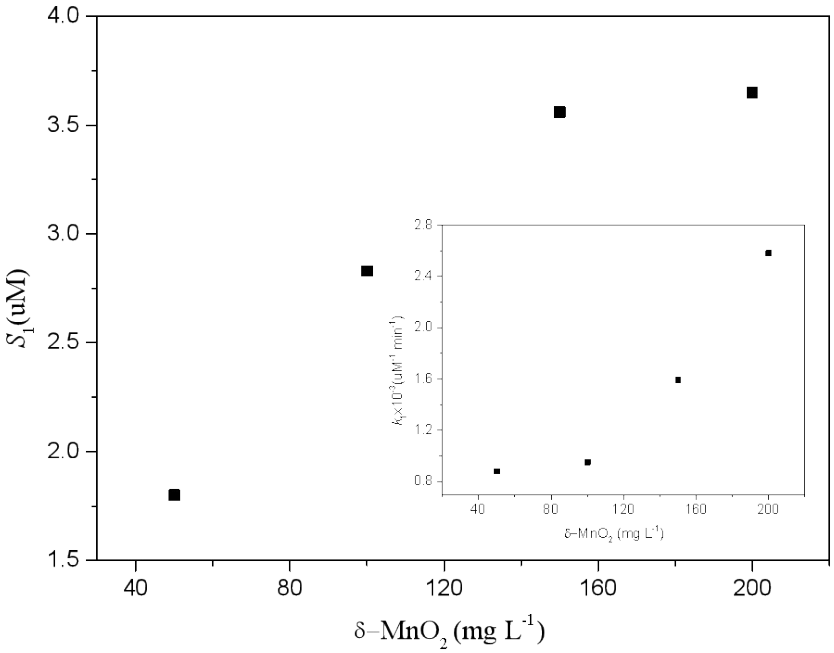

Fig. S6. Effect of δ-MnO_2 concentration on S_1 and k_1.

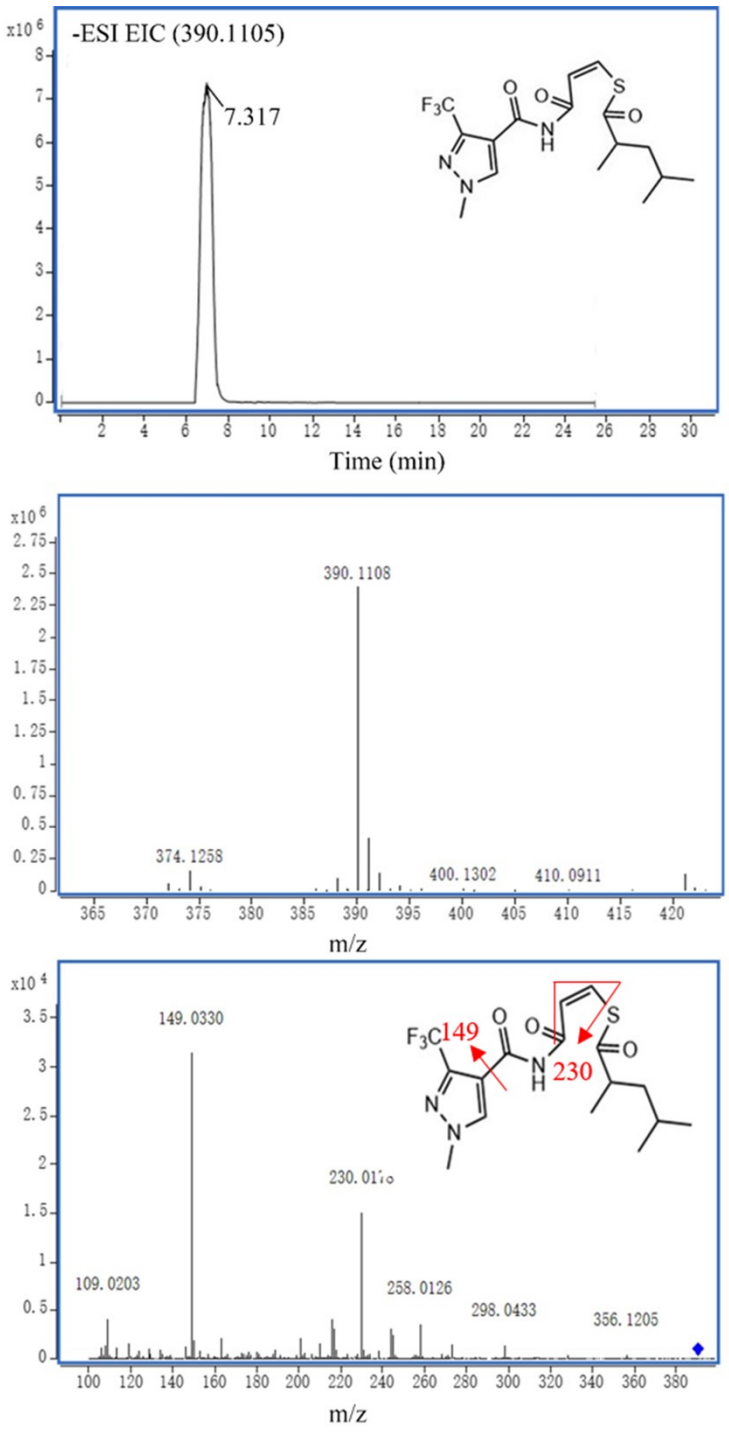

Fig. S7. Identification of P1 (m/z 390.1105) and its MS^1, MS^2 spectra.

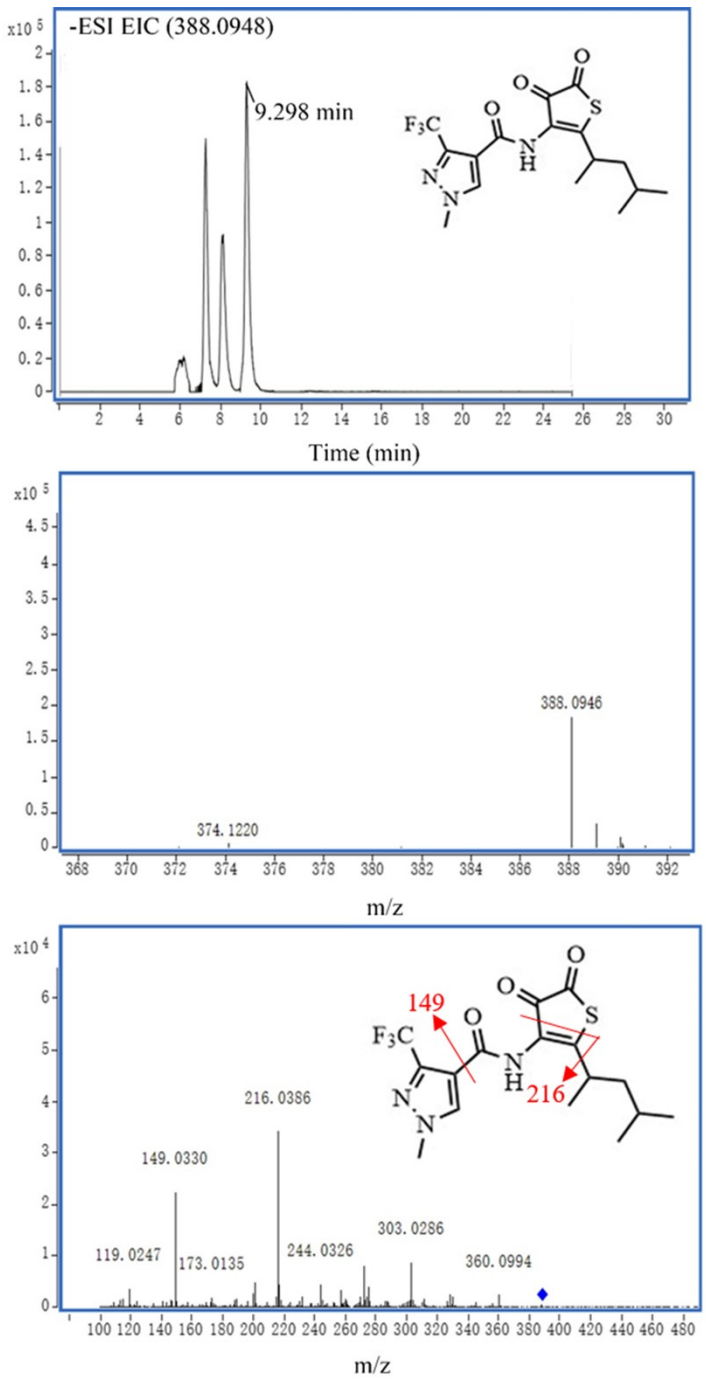

Fig. S8. Identification of P2 (m/z 388.0948) and its MS^1, MS^2 spectra.

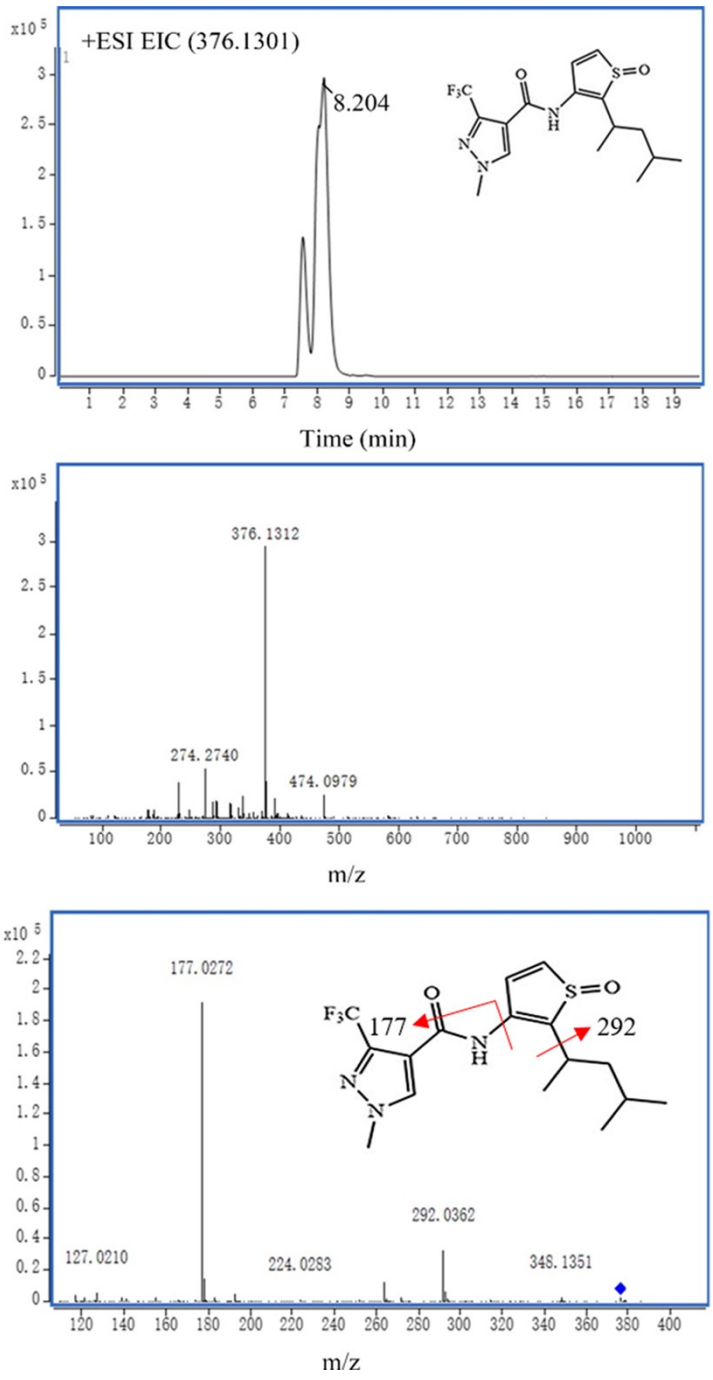

Fig. S9. Identification of P3 (m/z 376.1301) and its MS^1, MS^2 spectra.

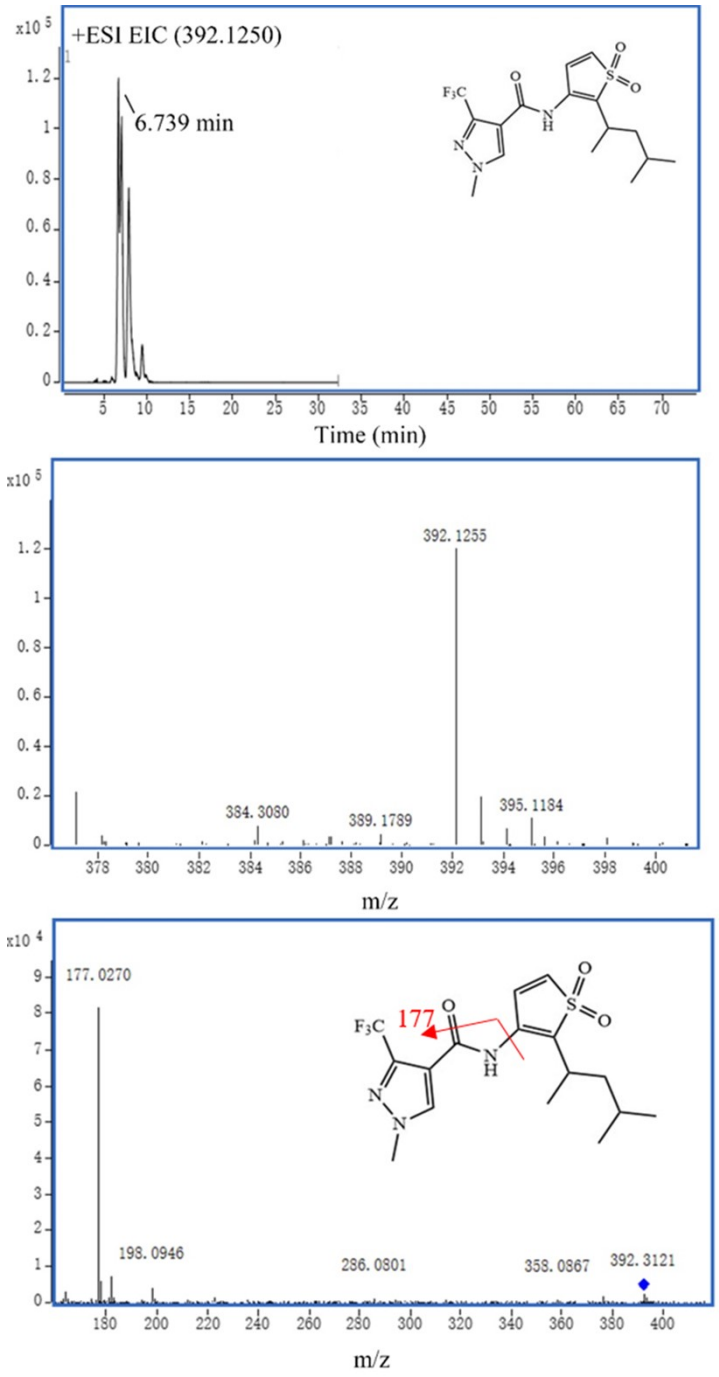

Fig. S10. Identification of P4 (m/z 392.1250) and its MS^1, MS^2 spectra.

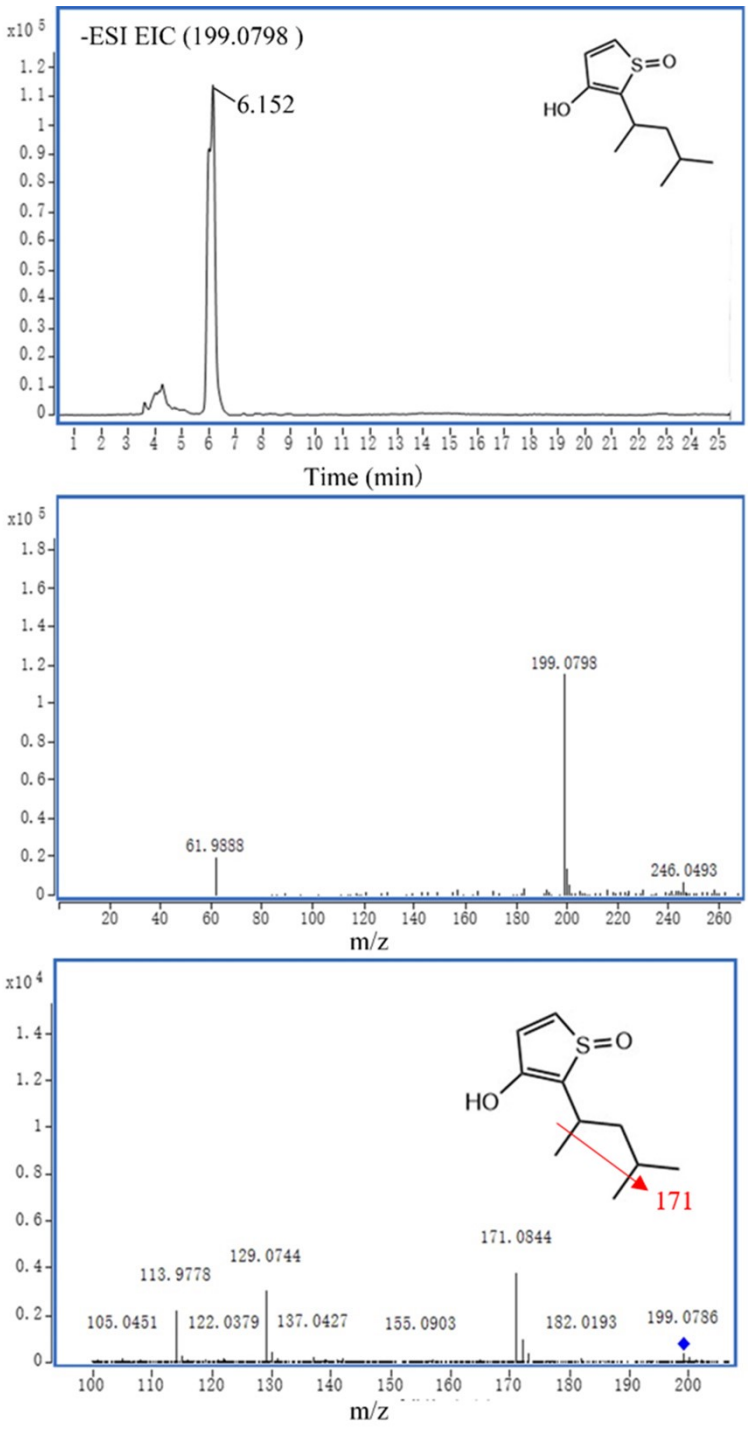

Fig. S11. Identification of P5 (m/z 199.0798) and its MS^1, MS^2 spectra.

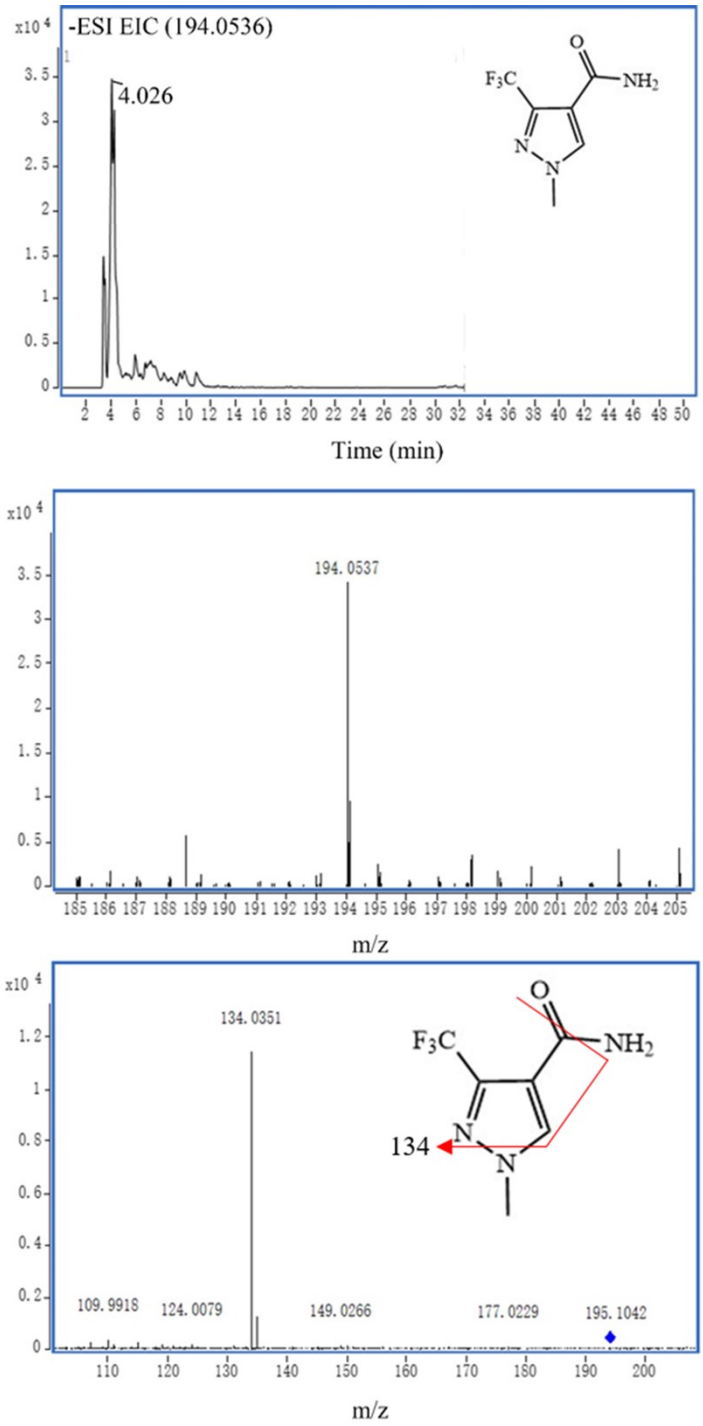

Fig. S12. Identification of P6 (m/z 194.0536) and its MS^1, MS^2 spectra.

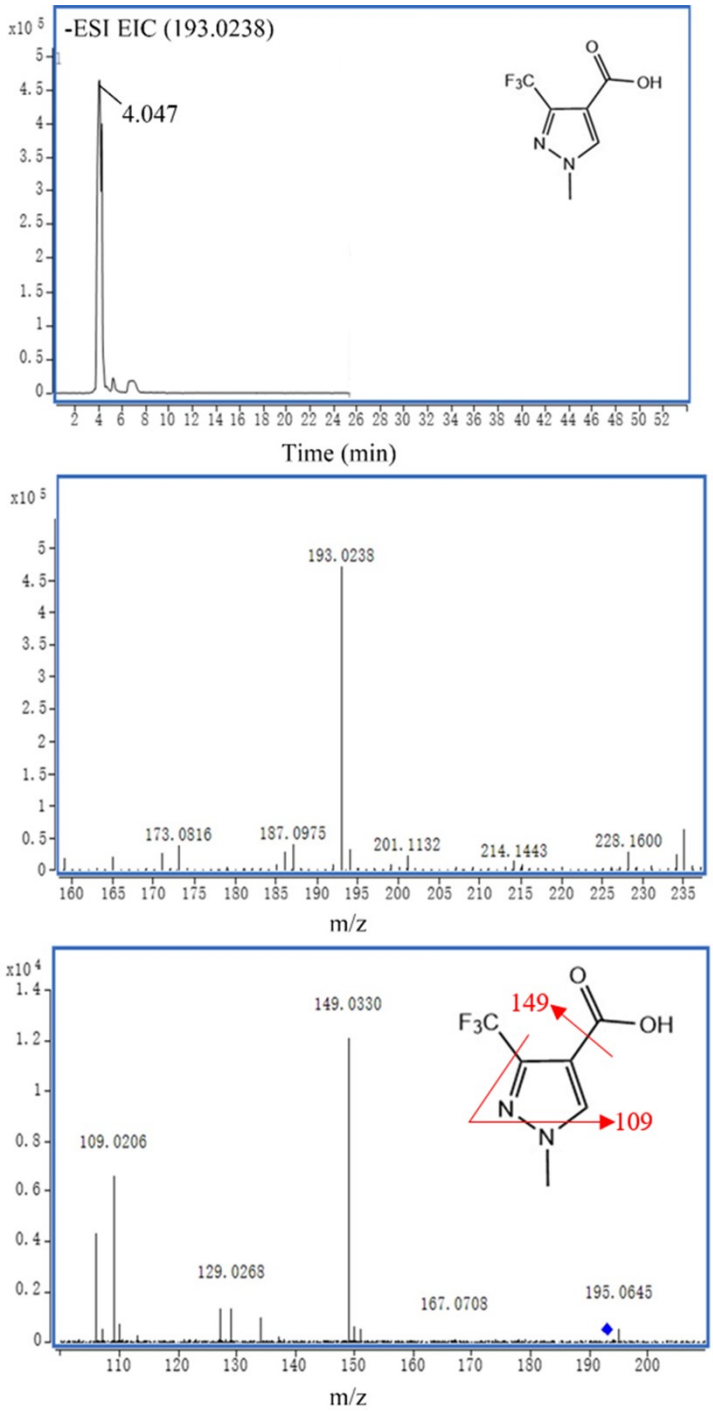

Fig. S13. Identification of P7 (m/z 193.0238) and its MS^1, MS^2 spectra.

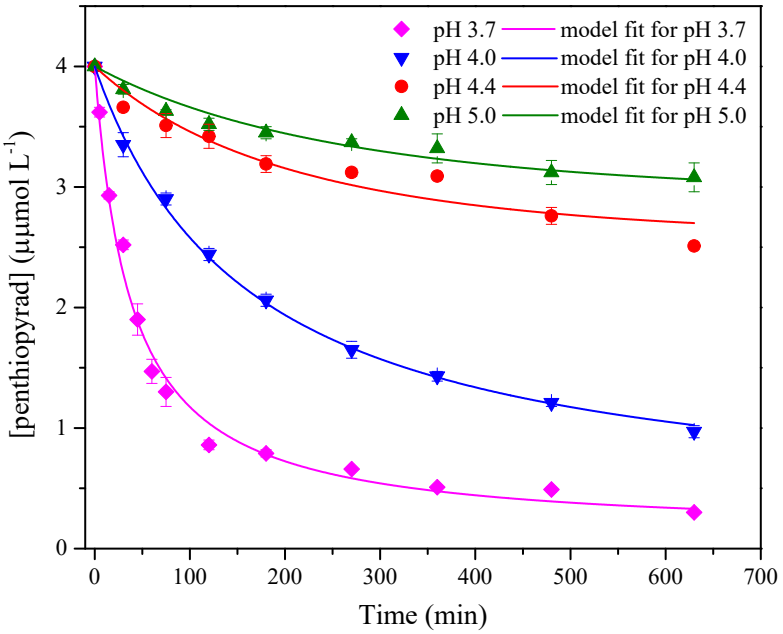

Fig. S14. Effect of solution pH on penthiopyrad degradation ($[penthiopyrad]_0$ = 4 μmol L^{-1}, $[\delta\text{-}MnO_2]_0$ = 150 mg L^{-1}, pH 3.7–5.0, $[NaCl]_0$ = 10 mmol L^{-1}).

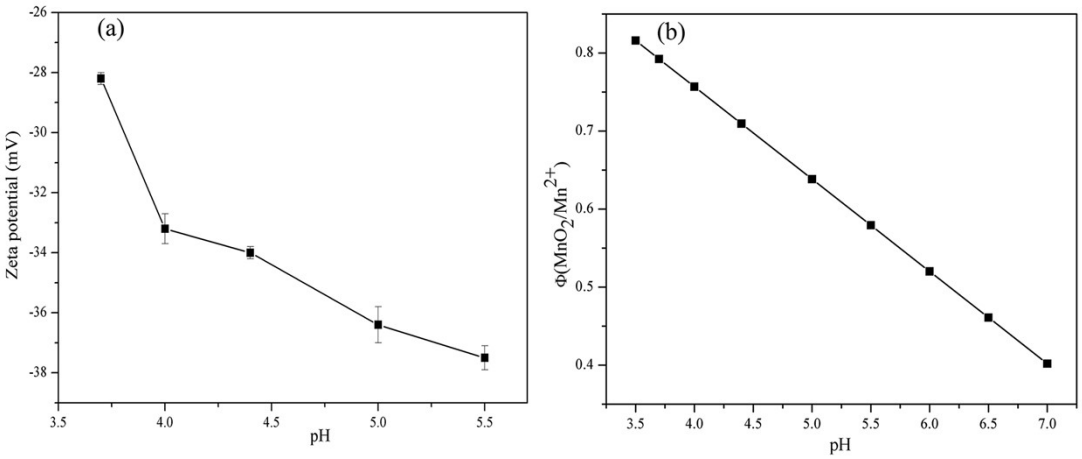

Fig. S15. (a) Zeta potential and the oxidation potential of $\delta\text{-}MnO_2$ in different solution pH. (b) the oxidation potential of $\delta\text{-}MnO_2$ in different solution pH.

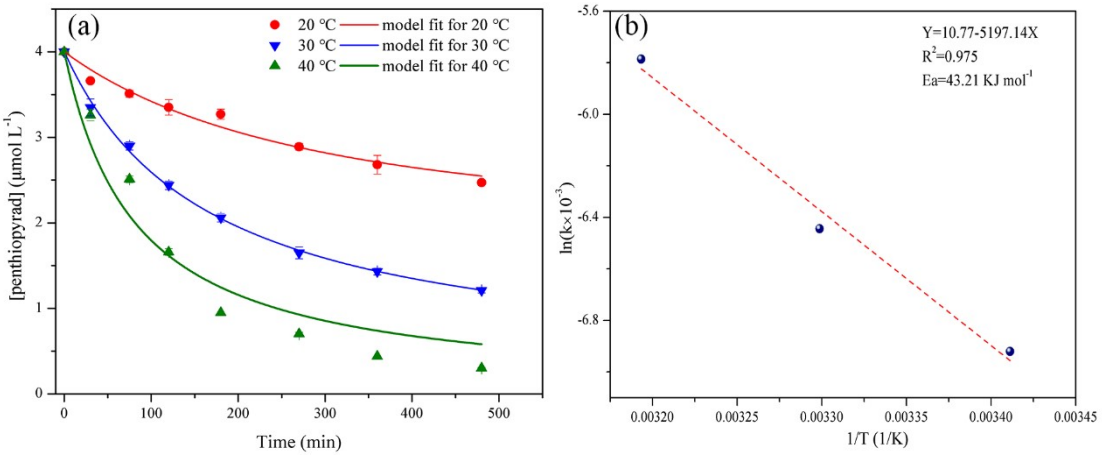

Fig. S16. Effect of temperature on penthiopyrad degradation ([penthiopyrad]$_0$ = 4 μmol L^{-1}, [δ-MnO_2]$_0$ = 150 mg L^{-1}, pH=4, [NaCl]$_0$ = 10 mmol L^{-1}); (b) Plot of k versus 1/T for activated energy calculation

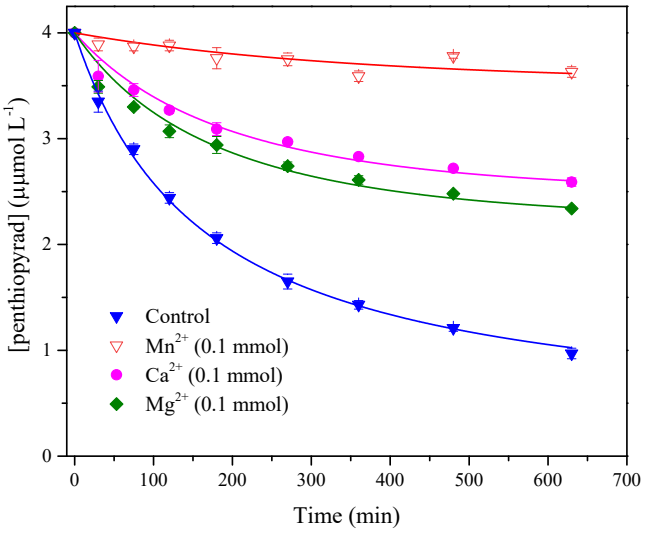

Fig. S17. Effect of metal cations on penthiopyrad degradation ([penthiopyrad]$_0$ = 4 μmol L^{-1}, [δ-MnO_2]$_0$ = 150 mg L^{-1}, pH=4, [NaCl]$_0$ = 10 mmol L^{-1}).

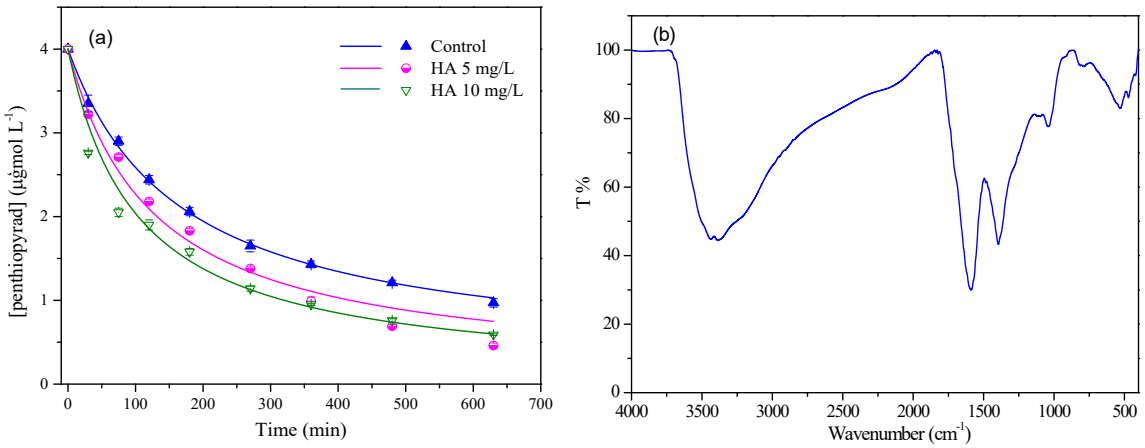

Fig. S18. (a) Effect of humic acid on penthiopyrad degradation ([penthiopyrad]$_0$ = 4 μmol L^{-1}, [δ-MnO_2]$_0$ = 150 mg L^{-1}, pH=4, [NaCl]$_0$ = 10 mmol L^{-1}). (b) FTIR spectra of the humic acid.

The Fig. S18b shown the FTIR spectra of the humic acid. The sharp peaks appearing in the band of 1132~700 cm^{-1} in the fingerprint area mainly correspond to the stretching vibrations of C-O in the carboxylic acid, alcohol, ester and phenolic hydroxyl groups. Combined with the C=O and aromatic ring structures appearing at 1705~1300 cm^{-1} and the elements in the element analysis high C and O content, which indicated that humic acid contained more carboxyl groups and phenolic hydroxyl groups.